JOURNAL OF MAGNETIC RESONANCE **129,** 53–66 (1997)
ARTICLE NO. MN971240

1D and 2D MAS NMR Spectra of a Dipolar-Coupled Homonuclear Spin-$\frac{1}{2}$ Pair

Enn Kundla, Ivo Heinmaa, Helgi Kooskora, and Endel Lippmaa

Institute of Chemical Physics and Biophysics, Akadeemia Tee 23, Tallinn EE0026, Estonia

Received February 7, 1997; revised July 17, 1997

An analytical approach based on the average Hamiltonian theory is proposed for efficient calculation of the MAS NMR spectra of a dipolar-coupled homonuclear spin-$\frac{1}{2}$ pair. For this purpose a superoperator formalism is developed which allows one to describe the spectra over a broad span of sample spinning rates, including the exact rotational resonances. This formalism can also be applied to the description of 2D polarization exchange spectra, which in many cases turns out to be useful for measuring the coupling strength. The experimental MAS NMR and the 2D spectra of doubly ^{13}C-labeled zinc acetate were found to be in good agreement with the calculated spectra. © 1997 Academic Press

INTRODUCTION

The magic angle spinning (MAS) technique in high field nuclear magnetic resonance (NMR), if applied to a rare spin-$\frac{1}{2}$ pair in powdered solids, yields spectra which display a number of special features absent in the spectra of samples containing dilute noncoupled spin-$\frac{1}{2}$ nuclei. Substantial broadenings and splittings of the resonance lines appear if a multiple of the sample spinning rate matches the difference between the resonance frequencies of the coupled nuclei. This phenomenon was observed first by Andrew *et al.* (*1*) and by now it is known as rotational resonance (*2–8*). Although the largest effects in the spectra appear at exact rotational resonances, the dependence of the lineshape on the sample spinning rate can occur also at spinning rates far from exact resonances (*6–13*). The extent of the effects depends upon the magnitudes of dipolar (DI), indirect spin–spin (SSI), and chemical shift interactions (CSI) of coupled nuclei as well as on the relative orientations of the tensor principal axis systems (PAS) of all these interactions. Therefore a detailed analysis of the lineshapes in the NMR spectra of paired nuclei can be used in structural studies of solids where isolated nuclear spin pairs exist either naturally or due to specific isotopic labeling (*5–13*). In order to reach the rotational resonance condition in case of limited sample spinning rates, various additional radiofrequency excitations during the evolution of the spin system have been suggested (*4, 10, 14–16*).

The lineshapes of a coupled spin-$\frac{1}{2}$ pair in a MAS NMR spectrum have been successfully simulated by Levitt *et al.* (*5*) by means of numerical calculations in which one sample rotation period was divided into a large number of small steps of duration Δt, during which the Hamiltonian may be assumed to be time independent. A good agreement between the experimental spectra and the calculated spectra was established this way, and the analytical formula of the lineshape was given for the case of vanishing CSI anisotropy. Similar results were obtained by Nakai and McDowell (*7*) and Schmidt and Vega (*8*) using Floquet theory (*17*). Such numerical calculations, however, need considerable computation time, especially to obtain the powder spectra, where typically 10^4 crystallite orientations must be taken into account.

The most popular approach in NMR, the average Hamiltonian theory (*18*) (AHT), was used in the case of the so-called zeroth-order rotational resonance, where the difference between the Larmor frequencies (Δ_L) of the two nuclei is zero or small compared to the rate of the sample rotation (*9–13*). It is clear that AHT cannot be applied in the traditional manner to the case of a coupled spin pair, if Δ_L is of the order of the rotation rate (ω_r) and the exact rotational resonance condition $p\omega_r = \Delta_L$, $p = 1, 2, \cdots$ is not fulfilled. Indeed, the first step in the traditional treatment is transformation of the Hamiltonian from the laboratory frame to the specific one, doubly rotating at Larmor frequencies of the individual nuclei. The next step, the procedure of averaging, unfortunately cannot be realized in a general case due to the complicated time dependence of the transformed Hamiltonian.

A modification of the average Hamiltonian approach recently proposed by us (*19*) allows one to describe the NMR lineshapes of a coupled spin-$\frac{1}{2}$ pair in experiments with arbitrary ratios between Δ_L and ω_r and including all the relevant interactions. This modification uses for the doubly rotating frame frequencies the corresponding multiples of ω_r. In the frame chosen this way the subsequent averaging can be car-

1090-7807/97 $25.00
Copyright © 1997 by Academic Press
All rights of reproduction in any form reserved.

ried out within the ordinary restrictions, while the small difference between the actual Larmor frequencies and the multiples of ω_r can be treated as small perturbations in the transformed Hamiltonian [see, e.g., Ref. (*20*)]. The main advantage of the AHT approach compared to the numerical methods is that it provides analytical formulae for the single-crystal resonance frequencies as well as the relative intensities. Thus the powder pattern simulations can be performed very efficiently. At this point we wanted to refer to the other efficient numerical simulation procedures recently proposed for rotational resonance. Edén *et al.* (*21*) have proposed an explicit time domain calculation, performed over a single modulation period, which is a much more efficient numerical algorithm than the Floquet approach. A similar efficient calculation routine using Floquet theory combined with perturbation treatment has been given recently by Nakai and McDowell (*22*), where the authors provide the recurrence formulae, making it possible to take into account high-order perturbation correction terms in the calculation.

In this report we demonstrate that the AHT-based effective Hamiltonian allows one to describe the evolution of the two-spin system state under arbitrary rotational resonance conditions analytically via a vector formalism in a 16-dimensional spin space. This formalism is handy for describing ordinary rotational resonance spectra, but it is particularly useful in getting the formulae for single-crystal line positions and relative intensities in more sophisticated experiments, e.g., 2D experiments, where the free evolution of the polarization vector is interrupted from time to time by strong RF pulses, because in this formalism the description of the polarization vector motion during free evolution intervals does not demand the use of a presentation diagonalizing the effective Hamiltonian. We will apply this approach to the study of 2D NMR spectra of polarization exchange. As was shown earlier (*23*), an effective polarization exchange between the coupled nuclei takes place at rotational resonance. Studying this effect in a 2D experiment may turn out to be a useful method for obtaining information about the coupling interactions in cases where the analysis of the powder lineshape is hindered by other overlapping lines in the 1D spectrum, e.g., if the spectrum contains lines from uncoupled spins.

The paper is organized as follows: In the next section we present the general ideology of the theory. In the third section we will compare the experimental one-dimensional spectra with the simulated spectra, and the analysis of the powder pattern in the presence of the CSI will be given. The fourth section is devoted to the description of the two-dimensional spectra.

GENERAL

In the following the high field MAS NMR spectra of a system of two spin-$\frac{1}{2}$ nuclei (I, S) will be treated. We proceed from the Hamiltonian which consists of six terms in the laboratory frame,

$$\mathbf{H} = \mathbf{H}_Z^{(I)} + \mathbf{H}_Z^{(S)} + \mathbf{H}_{CS}^{(I)} + \mathbf{H}_{CS}^{(S)} + \mathbf{H}_D + \mathbf{H}_J. \quad [1]$$

Here the isotropic components of the CSI of both nuclei are included in the corresponding Zeeman terms, i.e.,

$$\mathbf{H}_Z^{(F)} = -\omega_0^{(F)}(1 - \sigma^{(F)})\mathbf{F}_z \equiv -\omega_L^{(F)}\mathbf{F}_z, \quad \mathbf{F} = \mathbf{I}, \mathbf{S}, \quad [2]$$

and the Larmor frequencies $\omega_L^{(F)}$ relate to the frequencies of the bare nuclei $\omega_0^{(F)}$ through the trace of the corresponding CSI tensors

$$\sigma^{(F)} = \tfrac{1}{3}\mathrm{Tr}(\sigma^{(F)}), \quad F = I, S. \quad [3]$$

The chemical shift terms in Eq. [1] include the secular part of the anisotropic CSI

$$\mathbf{H}_{CS}^{(F)} = \omega_0^{(F)}\sigma_0^{(F)}\mathbf{F}_z, \quad \mathbf{F} = \mathbf{I}, \mathbf{S}, \quad [4]$$

where the screening tensor components are defined as

$$\sigma_0^{(F)} = \sigma_{zz}^{(F)} - \sigma^{(F)}. \quad [5]$$

The DI term is taken in the truncated form

$$\mathbf{H}_D = \omega_D D_0[\mathbf{I}_z\mathbf{S}_z - \tfrac{1}{4}(\mathbf{I}_+\mathbf{S}_- + \mathbf{I}_-\mathbf{S}_+)], \quad [6]$$

where

$$\omega_D = \gamma^{(I)}\gamma^{(S)}\hbar^2/r^3 \quad [7]$$

and γ denotes the gyromagnetic ratio and r is the distance between the nuclei I and S. The last term in Eq. [1] takes into account the isotropic SSI between the nuclei in the pair

$$\mathbf{H}_J = \omega_J[\mathbf{I}_z\mathbf{S}_z + \tfrac{1}{2}(\mathbf{I}_+\mathbf{S}_- + \mathbf{I}_-\mathbf{S}_+)]. \quad [8]$$

Due to mechanical rotation of the sample, the laboratory frame components of the screening and dipolar tensors depend harmonically on time,

$$\sigma_0^{(F)} = \sum_{n=-2}^{2} \sigma_{0,n}^{(F)}(\delta, \eta, \lambda, \mu, \nu, \alpha, \beta, \gamma)e^{in\omega_r t}, \quad F = I, S$$

$$D_0 = \sum_{n=-2}^{2} D_{0,n}(\alpha, \beta, \gamma)e^{in\omega_r t}. \quad [9]$$

Here the chemical shift anisotropy δ and asymmetry η are defined in the shielding tensor principal axes system in the usual manner,

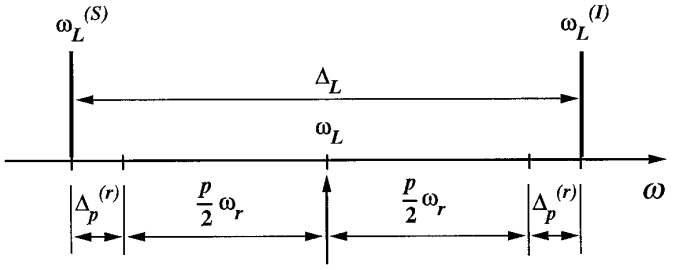

FIG. 1. Schematic illustration of the notation in the sample spinning rate depending on transformation $\mathbf{T}$.

$$\delta = \sigma_{zz}^{(\mathrm{PAS})} - \sigma,$$
$$\eta = (\sigma_{yy}^{(\mathrm{PAS})} - \sigma_{xx}^{(\mathrm{PAS})})/\delta. \qquad [10]$$

The Eulerian angles λ, μ, and ν describe the orientation of the chemical shift tensor PAS relative to the molecule-fixed coordinate system, which hereafter is taken with the z-axis along the line connecting the two nuclei. The Eulerian angles α, β, and γ determine the orientation of this molecule-fixed coordinate system in a single crystal relative to a rotor-fixed frame in which the z-axis is oriented along the rotation axis and tilted at the magic angle from the external magnetic field direction.

In the high field experiments $\omega_{\mathrm{L}}^{(I)}$ and $\omega_{\mathrm{L}}^{(S)}$ greatly predominate over all the other amplitudes and frequencies in the Hamiltonian Eq. [1]. It is reasonable to choose for further analysis another representation in which the influence of Zeeman terms is suitably reduced. It appears that one of the most useful possibilities for that is to use the sample spinning rate-dependent transformation according to the definitions

$$\mathbf{Q}_{\mathrm{T}} = \mathbf{T}^{-1}\mathbf{Q}\mathbf{T}^{1},$$
$$\mathbf{T}^{\pm 1} = \exp\left\{\pm it\left[\left(\omega_{\mathrm{L}} + \frac{p}{2}\omega_{\mathrm{r}}\right)\mathbf{I}_z + \left(\omega_{\mathrm{L}} - \frac{p}{2}\omega_{\mathrm{r}}\right)\mathbf{S}_z\right]\right\}. \qquad [11]$$

The transformation of Eq. [11] is illustrated by the sketch in Fig. 1. The notations in it have the following meaning:

$$\omega_{\mathrm{L}} = \tfrac{1}{2}(\omega_{\mathrm{L}}^{(I)} + \omega_{\mathrm{L}}^{(S)}), \qquad [12]$$
$$\Delta_{\mathrm{L}} = \omega_{\mathrm{L}}^{(I)} - \omega_{\mathrm{L}}^{(S)}, \qquad [13]$$

and the value of integer p, i.e., the order of the actual realized rotational resonance, is determined by the conditions

$$\Delta_{\mathrm{L}} = p\omega_{\mathrm{r}} + 2\Delta_p^{(r)}, \quad -\tfrac{1}{4}\omega_{\mathrm{r}} < \Delta_p^{(r)} < \tfrac{1}{4}\omega_{\mathrm{r}}. \qquad [14]$$

The transformation above leads to some kind of symmetry relative to the parameters of nuclei I and S, and, what particularly matters, it preserves the exact periodicity in time (frequency ω_{r}) of the transformed Hamiltonian. The latter quality allows one to form for the problem at hand an effective Hamiltonian by averaging over the sample spinning period ω_{r}^{-1} with ordinary restrictions (*18, 20*). At the averaging procedure we confine ourselves to two steps; i.e., we choose the effective Hamiltonian $\mathbf{H}^{(p)}$ as the sum of two terms

$$\mathbf{H}^{(p)} = \mathbf{H}_p^{(0)} + \mathbf{H}_p^{(1)}, \qquad [15]$$

where $\mathbf{H}_p^{(1)}$ takes into account the first-order correction from the time-dependent terms to the average value of the transformed Hamiltonian $\mathbf{H}_p^{(0)}$. This procedure is justified if

$$\omega_{\mathrm{r}} \gg \omega_{\mathrm{D}}, \omega_{\mathrm{J}}. \qquad [16]$$

It is immediately apparent that the general structure of the effective Hamiltonian,

$$\mathbf{H}^{(p)} = -\Delta_{\mathrm{Z}}^{(p)}\mathbf{I}_{\mathrm{Z}} + \Delta_{\mathrm{Z}}^{(p)}\mathbf{S}_{\mathrm{Z}} + \omega_{\mathrm{J}}\mathbf{I}_{\mathrm{Z}}\mathbf{S}_{\mathrm{Z}} - K_p\mathbf{I}_+\mathbf{S}_- - K_p^*\mathbf{I}_-\mathbf{S}_+, \qquad [17]$$

does not depend on the actual value of the coefficient p, whereas the amplitudes of the effective Hamiltonian terms

$$\Delta_{\mathrm{Z}}^{(p)} = \Delta_p^{(r)} + \Delta_p^{(i)}, \qquad [18]$$

where $\Delta_p^{(r)}$ is given by Eq. [14],

$$\Delta_p^{(i)} = \omega_{\mathrm{D}}^2 \sum_{\substack{n=-2 \\ n\neq 0,p}}^{2} [16(p-n)\omega_{\mathrm{r}}]^{-1} D_{0,n}D_{0,-n} + \omega_{\mathrm{J}}^2(4p\omega_{\mathrm{r}})^{-1}(1-\delta_{p,0}), \qquad [19]$$

$\delta_{p,0}$ is the Kronecker delta, and

$$K_p = \frac{1}{4}\omega_{\mathrm{D}}\left[D_{0,p} + \frac{1}{\omega_{\mathrm{r}}}\sum_{\substack{n=-2 \\ n\neq 0,p}}^{2}\frac{1}{n}(\omega_{\mathrm{L}}^{(I)}\sigma_{0,n}^{(I)} - \omega_{\mathrm{L}}^{(S)}\sigma_{0,n}^{(S)})D_{0,p-n}\right] - \frac{1}{2}\omega_{\mathrm{J}} \times \left[\delta_{p,0} + \frac{1}{p\omega_{\mathrm{r}}}(\omega_{\mathrm{L}}^{(I)}\sigma_{0,p}^{(I)} - \omega_{\mathrm{L}}^{(S)}\sigma_{0,p}^{(S)})(1-\delta_{p,0})\right] \qquad [20]$$

must be calculated for any particular value of p.

As soon as the effective Hamiltonian is known, the evolution of the spin system state can be determined by solution of the Liouville equation

$$\rho_T(t) = e^{-it\mathbf{H}^{(p)}}\rho_T(0)e^{it\mathbf{H}^{(p)}}, \quad [21]$$

in the presentation of Eq. [11].

The density operator ρ may be examined as the state vector in a 16-dimensional spin space and, in accordance with this, Eq. [21] as the formal description determining the motion of the state vector in the course of experiment. Thus the full analytical description of the spin system state evolution is always available independent of the realized value of p and the initial state $\rho(0)$ if only the formal law of Eq. [21] is specified for all the independent spin-space components. With the Hamiltonian of the form Eq. [17] this procedure is possible and the detailed expressions, describing the motion of the polarization vector, i.e., the evolution of the state vector in the spin space, are presented in the Appendix.

It is remarkable that the full 16-dimensional spin space is made up of four subspaces, in each of which the polarization vector evolves independently; i.e., the vector components of different subspaces do not mix under the $\mathbf{H}^{(p)}$-governed evolution. Moreover, there is a subspace (see [A8] and [A9] in the Appendix) where the evolution does not take place at all. In the other subspaces the polarization exchange between the nuclei I and S takes place. The fastest polarization exchange occurs in the third subspace [A6]. At that the polarization vector motion does not depend on isotropic SSI (a weak indirect dependence appears only through the amplitudes $\Delta_Z^{(p)}$ and K_p) unlike the case in the first and the second subspaces, where SSI contributes directly to the frequencies.

Naturally, an analytical description of the spin state evolution is useful for the analysis of ordinary rotational resonance experiments as it links the spectral parameters to the single-crystal internal interactions, but the main goal of a full analytical description of polarization vector evolution is found in the design and interpretation of experiments consisting of more than one evolution period under the rotational resonance conditions.

In the following section we apply the theory to the ordinary rotational resonance spectra.

ORDINARY MAS NMR SPECTRA OF A COUPLED PAIR OF SPIN-$\frac{1}{2}$ NUCLEI

Signal Expression

In this section we treat the experiments in which the NMR signal in a receiver coil directed along the x-axis is registered right after the generation of the polarization vector component in the xy-plane of the laboratory frame

$$\rho(0) \propto a(\mathbf{I}_+ + \mathbf{I}_-) + b(\mathbf{S}_+ + \mathbf{S}_-). \quad [22]$$

Note that the possible existence of z-components of the initial vector $\rho(0)$ is unimportant in the present case since they do not give rise to matrix elements which produce a signal in the receiver coil-selected subspace. The signal from a spin pair in the powder sample is calculated by the formula

$$S \propto \sum_{l,m=\pm 1} \left\{ a\left(1 + l\frac{\Delta_Z^{(p)}}{\Delta_p}\right)\cos\left[\left(\omega_L^{(I)} - \Delta_p^{(r)} + l\Delta_p + m\frac{1}{2}\omega_J\right)t\right] + b\left(1 - l\frac{\Delta_Z^{(p)}}{\Delta_p}\right) \times \cos\left[\left(\omega_L^{(S)} + \Delta_p^{(r)} + l\Delta_p + m\frac{1}{2}\omega_J\right)t\right]\right\}, \quad [23]$$

where

$$\Delta_p = \sqrt{(\Delta_Z^{(p)})^2 + K_p K_p^*}. \quad [24]$$

In Eq. [23] we have considered that the phase distortions in the signal from the single crystal (*5*, *19*) are canceled out in a powder sample where one always has a pair of crystallites oriented at angles (β, γ) and $(180° - \beta, 180° + \gamma)$ in the rotor-fixed frame.

Both the effective Hamiltonian given in Eq. [17] with Eqs. [18]–[20] and the expression for a single-crystal signal show that every MAS NMR experiment of a coupled spin pair belongs to one of the six possible regions (*19*), depending on the actual value of p. The parameters K_p and $\Delta_p^{(i)}$ at different p are collected in the Table 1, where the components of the dipolar tensor at MAS are

$$D_{0,\pm 1} = \mp i\frac{\sqrt{2}}{2}\sin 2\beta,$$
$$D_{0,\pm 2} = \frac{1}{2}\sin^2\beta \quad [25]$$

and we have taken the molecule-fixed frame coordinate with the z-axis along the line connecting the two nuclei. The components of the CSI tensor for the I and S nuclei $\sigma_{0,\pm k}$, $k = 1, 2$, can be obtained by transforming the chemical shift tensors in the appropriate way,

$$\sigma^{(F,\mathrm{PAS})} \xrightarrow{(\lambda^F,\mu^F,\nu^F)} \sigma^{(F,\mathrm{molecule})} \xrightarrow{(\alpha,\beta,\gamma)} \sigma^{(F,\mathrm{rotor})} \xrightarrow{(\theta)} \sigma^{(F,\mathrm{lab})}, \quad F = I, S,$$

where θ is the magic angle. As given in the Table 1 [see also Ref. (*19*)], the experiments at high rotation rates ($p = 0$) may be classified as a pure homonuclear case, since the Larmor frequencies of both nuclei are not distinguishable on the scale of ω_r as the measuring unit. Nevertheless an

TABLE 1
Interaction Parameters at *p*th Rotational Resonance

p	ω_r	K_p, $\Delta_p^{(i)}$
0	$\omega_r > 2\Delta_L$	$K_0 = \frac{\omega_D}{16\omega_r}\{[\omega_L^{(I)}(\sigma_{0,2}^{(I)} - \sigma_{0,-2}^{(I)}) - \omega_L^{(S)}(\sigma_{0,2}^{(S)} - \sigma_{0,-2}^{(S)})]\sin^2\beta + i2\sqrt{2}[\omega_L^{(I)}(\sigma_{0,1}^{(I)} + \sigma_{0,-1}^{(I)}) - \omega_L^{(S)}(\sigma_{0,1}^{(S)} + \sigma_{0,-1}^{(S)})]\sin 2\beta\} - \frac{1}{2}\omega_J.$
		$\Delta_0^{(i)} = 0.$
1	$\frac{2}{3}\Delta_L < \omega_r < 2\Delta_L$	$K_1 = \frac{\omega_D}{8}\left\{-i\sqrt{2}\sin 2\beta + \frac{1}{\omega_r}\left[-(\omega_L^{(I)}\sigma_{0,-1}^{(I)} - \omega_L^{(S)}\sigma_{0,-1}^{(S)})\sin^2\beta + i\frac{\sqrt{2}}{2}(\omega_L^{(I)}\sigma_{0,2}^{(I)} - \omega_L^{(S)}\sigma_{0,2}^{(S)})\sin 2\beta\right]\right\}$
		$- \frac{\omega_J}{2\omega_r}(\omega_L^{(I)}\sigma_{0,1}^{(I)} - \omega_L^{(S)}\sigma_{0,1}^{(S)}).$
		$\Delta_1^{(i)} = \frac{\omega_D^2}{16\omega_r}\left(\sin^2\beta - \frac{7}{6}\sin^4\beta\right) + \frac{\omega_J^2}{4\omega_r}.$
2	$\frac{2}{5}\Delta_L < \omega_r < \frac{2}{3}\Delta_L$	$K_2 = \frac{\omega_D}{8}\left[\sin^2\beta - i\frac{\sqrt{2}}{\omega_r}(\omega_L^{(I)}\sigma_{0,1}^{(I)} - \omega_L^{(S)}\sigma_{0,1}^{(S)})\sin 2\beta\right] - \frac{\omega_J}{4\omega_r}(\omega_L^{(I)}\sigma_{0,2}^{(I)} - \omega_L^{(S)}\sigma_{0,2}^{(S)}).$
		$\Delta_2^{(i)} = \frac{\omega_D^2}{6\omega_r}\left(\sin^2\beta - \frac{125}{128}\sin^4\beta\right) + \frac{\omega_J^2}{8\omega_r}.$
3	$\frac{2}{7}\Delta_L < \omega_r < \frac{2}{5}\Delta_L$	$K_3 = \frac{\omega_D}{8\omega_r}\left[(\omega_L^{(I)}\sigma_{0,1}^{(I)} - \omega_L^{(S)}\sigma_{0,1}^{(S)})\sin^2\beta - i\frac{\sqrt{2}}{2}(\omega_L^{(I)}\sigma_{0,2}^{(I)} - \omega_L^{(S)}\sigma_{0,2}^{(S)})\sin 2\beta\right].$
		$\Delta_3^{(i)} = \frac{3\omega_D^2}{32\omega_r}(\sin^2\beta - \frac{4}{5}\sin^4\beta) + \frac{\omega_J^2}{12\omega_r}.$
4	$\frac{2}{9}\Delta_L < \omega_r < \frac{2}{7}\Delta_L$	$K_4 = \frac{\omega_D}{16\omega_r}(\omega_L^{(I)}\sigma_{0,2}^{(I)} - \omega_L^{(S)}\sigma_{0,2}^{(S)})\sin^2\beta.$
		$\Delta_4^{(i)} = \frac{\omega_D^2}{15\omega_r}\left(\sin^2\beta - \frac{27}{32}\sin^4\beta\right) + \frac{\omega_J^2}{16\omega_r}.$
≥ 5	$\omega_r < \frac{2}{9}\Delta_L$	$K_{\geq 5} = 0.$
		$\Delta_p^{(i)} = \frac{\omega_D^2}{32\omega_r}\left(\frac{2p}{p^2-1}\sin^2 2\beta + \frac{p}{p^2-4}\sin^4\beta\right) + \frac{\omega_J^2}{4p\omega_r}.$

effective coupling between the spins exists ($K_0 \neq 0$). The strongest coupling between the two spins occurs in cases $p = 1$ and $p = 2$. Here the effective coupling includes the pure scaled dipolar interaction, the cross-effect of dipolar and anisotropic CSI of both nuclei, and the cross-effect of isotropic SSI and anisotropic CSI. At lower rotation rates ($p = 3$ and $p = 4$) the effective coupling is weaker and is made up solely by the cross-effect of DI and CSI anisotropy. Experiments at the lowest rotation rates ($p \geq 5$) may be regarded as the case of heteronuclear coupling. Here the coupling between spins caused by anisotropic interactions vanishes ($K_p = 0$). It is clear that the most complicated powder lineshapes are expected at the rotation rates around the first and the second rotational resonances, corresponding to the cases $p = 1$ and $p = 2$. These cases are obviously the most difficult ones for the applicability of the theory. On the other hand, this region of rotation rates is definitely the most useful one for structural studies.

Experimental

The calculated spectra are compared with the experimental ^{13}C MAS NMR spectra of ^{13}C in highly enriched solid Zn-acetate, $Zn(CH_3COO)_2$. This compound has a useful structure with only two magnetically different sites for carbon, and the 4.1% of ^{67}Zn nuclei ($I = \frac{5}{2}$) possessing a low gyromagnetic ratio have only a very minor effect on the neighboring carboxyl carbon (COO) resonance. The sample

of ^{13}C doubly labeled $Zn(^{13}CH_3{}^{13}COO)_2$ was synthesized from the 99.9% ^{13}C doubly labeled acetic acid (Aldrich). NMR measurements were performed on a Bruker CXP-200 spectrometer operating at 50.31 MHz for ^{13}C NMR in a 4.7-T external magnetic field. A homebuilt MAS probehead designed for a 4-mm rotor diameter allowed us to use sufficiently fast sample spinning rates. The spectra were obtained by the conventional cross-polarization and proton decoupling technique. Usually two FIDs at a constant sample spinning frequency were accumulated. The instability of the spinning frequency during the two scans did not exceed 1 Hz. The frequency shifts in Figs. 2 and 4 are measured with respect to the resonance frequency of the methyl carbon in natural abundant Zn-acetate at 23.7 ppm from TMS.

The numerical calculations were performed at a Gateway 2000 4DX2-66V computer. Typically 10^4 crystallite orientation were taken into account in the simulation of the powder patterns. The computation time of 1D spectrum was about 20 s.

Lineshapes at the First Rotational Resonance

In Fig. 2a we show the comparison of the calculated (full lines) and observed (dotted lines) ^{13}C MAS NMR spectra from methyl carbon sites of Zn-acetate. The actual parameters for the homonuclear $^{13}C-{}^{13}C$ pair in Zn-acetate were taken from Ref. (*5*). A uniform residual Lorentzian half-width of 20 Hz was convoluted in the calculated spectra. In Fig. 2b the calculated spectra are shown without this additional broadening. As one can see the spectrum consists of two bands of equal width. At exact resonance ($\nu_r = 8.03$ kHz) the two bands have about equal intensities and shapes. At higher or lower sample spinning rates one of the bands (the main band) remains located close to the Larmor frequency of that nucleus and the other band is separated from the main band by a frequency equal to the offset $\Delta_L - p\omega_r$ from the exact rotational resonance. With increasing offset the widths of the bands decrease and the intensity of the second band decreases. At large offset values the second band is outside the frequency range given in the figure. Comparison of the experimental and calculated spectra demonstrates that agreement is surprisingly good over the whole observed range of sample spinning rates.

We now proceed to analyze the powder patterns at exact resonance in the presence of CSI. In Fig. 3 we have shown typical powder patterns at the first rotational resonance. For clarity we ignored here the SSI, taking $\omega_J = 0$. In the case of vanishing CSI the powder pattern is relatively simple (Fig. 3a), showing the two singular peaks at frequency $\Delta_{10} = \pm\sqrt{2}\omega_D/8$ [see Refs. (*5, 19*)]. The effect of CSI on the lineshape depends on the magnitudes and mutual orientations of the DI and CSI tensors. In order to analyze the effect we have confined ourselves to the case where only one of the nuclei, (I), in the pair has substantial anisotropy of the

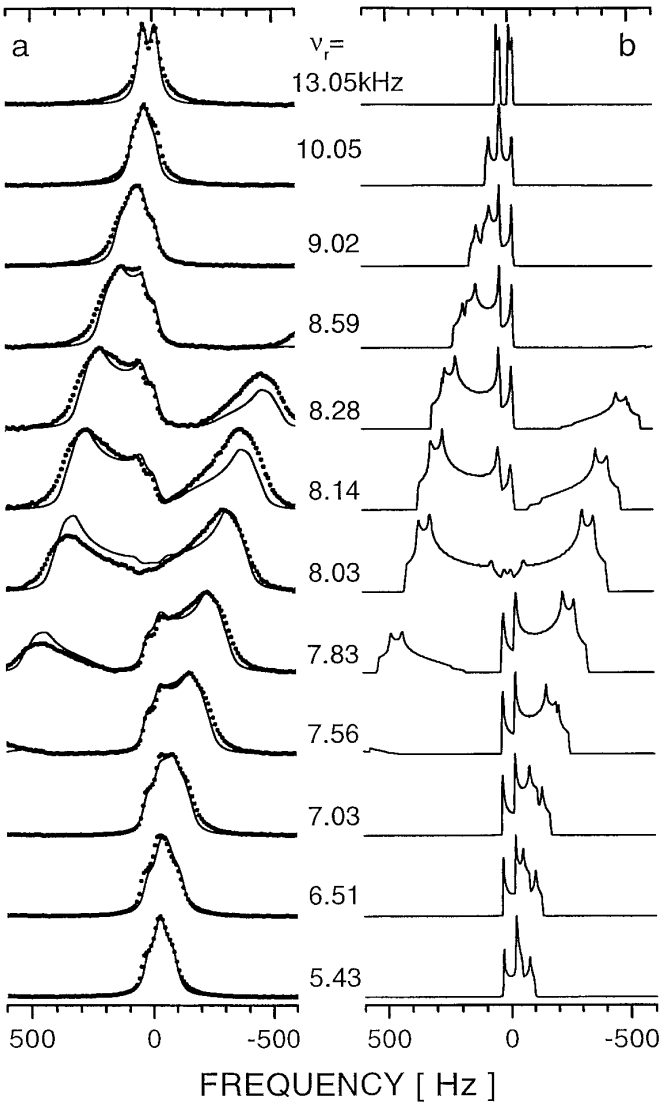

FIG. 2. ^{13}C MAS NMR spectra of the methyl carbon in solid 99.9% ^{13}C-enriched Zn-acetate as a function of sample spinning frequency ν_r around the first rotational resonance. The following parameters were used: $\omega_L/2\pi = 50.31$ MHz, $\Delta_L/2\pi = 8030$ Hz and $\omega_J/2\pi = 52$ Hz, $\omega_D/2\pi = 2000$ Hz, the chemical shift anisotropy for the CH_3 carbon $\delta^{(S)} = 23$ ppm, asymmetry $\eta^{(S)} = 0.17$, with PAS oriented at Euler angles with respect to the molecule-fixed frame $(\lambda^S, \mu^S, \nu^S) = (0, 0, 0)$; corresponding parameters for the carboxyl site, COO: $\delta^{(I)} = 79$ ppm, $\eta^{(I)} = 0.34$ and $(\lambda^I, \mu^I, \nu^I) = (0, \pi/2, 0)$. (a) Observed (dotted lines) and calculated (full lines) spectra. A common Lorentzian half-width of 20 Hz was convoluted in the calculated spectra. (b) Calculated spectra without additional broadening.

CSI with $\eta^{(I)} = 0$. In this case it is possible to provide analytical formulae for the positions of the singular points in the powder pattern for two basic mutual orientations of the CSI and DI tensors $\mu = 0$ and $\mu = 90°$, which might be useful for the estimates.

In the $\mu = 0$ case (see Fig. 3b) the powder pattern is very similar to the case of vanishing CSI, showing two singular peaks at $\pm\Delta_{1a}$. Using the parameters

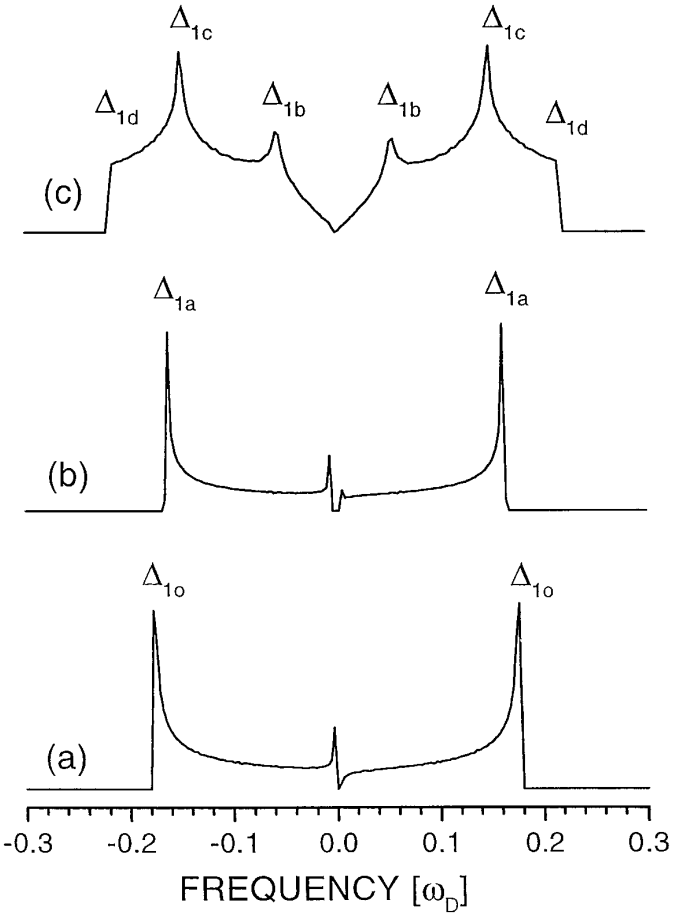

FIG. 3. Typical powder patterns (in units of ω_D) of the coupled spin-$\frac{1}{2}$ pair exactly at the first rotational resonance depending on the mutual orientation of the CSI and DI tensors. Positions of the noted singularities are given in the text. The model parameters: $\Delta_L/2\pi = 8.0$ kHz, $\omega_D/2\pi = 2.0$ kHz, $\eta^{(I)} = 0$, $\delta^{(S)} = 0$, $\omega_J = 0$. (a) $\delta^{(I)} = 0$; (b) $\delta^{(I)} = 200$ ppm, $\mu^{(I)} = 0$; (c) $\delta^{(I)} = 200$ ppm, $\mu^{(I)} = \pi/2$.

$$c = \frac{\omega_L \delta}{\Delta_L},$$

$$d = \frac{2\omega_D}{3\Delta_L}, \qquad [26]$$

where δ is the only relevant anisotropy of the CSI, the singular peak position can be evaluated as

$$\Delta_{1a} = \left| \frac{\sqrt{2}}{8}\,\omega_D \sqrt{\left[1 - \frac{c}{16}(1 + \xi_a)\right]^2 (1 - \xi_a^2) + \left(\frac{\sqrt{2}d}{64}\right)^2 (5 - 7\xi_a)^2 (1 + \xi_a^2)} \right|, \qquad [27]$$

where

$$\xi_a = [16 - c - \sqrt{(16 - c)^2 + 8c^2}]/4c. \qquad [28]$$

At moderate values of the CSI anisotropy, $|c| \leq 2$,

$$\Delta_{1a} \cong \left| \frac{\sqrt{2}}{8}\,\omega_D \frac{16}{16 + c} \right|. \qquad [29]$$

In the $\mu = 90°$ case the singular points in the powder pattern have the following positions:

$$\Delta_{1b} = \left| \frac{\sqrt{2}}{8}\,\omega_D \frac{1}{4} \sqrt{c^2 + \frac{1}{8} d^2} \right|, \qquad [30]$$

$$\Delta_{1c} = \left| \frac{\sqrt{2}}{8}\,\omega_D \sqrt{\left(1 - \frac{1}{8} c\right)^2 + 2\left(\frac{5d}{64}\right)^2} \right|. \qquad [31]$$

The last singularity exists in the range $-32 \leq c \leq 8$,

$$\Delta_{1d} = \left| \frac{\sqrt{2}}{8}\,\omega_D \left[1 + \frac{c}{16}(3 + \xi_d)\right] \sqrt{1 - \xi_d^2} \right|, \qquad [32]$$

where

$$\xi_d = [-(3c + 16) + \sqrt{(3c + 16)^2 + 8c^2}]/4c, \qquad [33]$$

and the singularity exists in the range $-4 \leq c \leq \infty$. Here we must add that the singularity at Δ_{1c} is a peak in the powder pattern if $\delta > 0$ or the most shifted shoulder if $\delta < 0$ and, similarly, the singularity at Δ_{1d} is the most shifted shoulder if $\delta > 0$ and the peak if $\delta < 0$. Additional singularities appear in the powder pattern if the absolute value of the parameter c (the CSI anisotropy) becomes larger, $c < -4$, or $c \geq 8$, but for such cases it will be more convenient to find the powder pattern from the simulation.

Lineshapes at the Second Rotational Resonance

A similar comparison of the calculated and recorded Zn-acetate lineshapes was made for sample spinning speeds around the second rotational resonance which occurs at $\omega_r/2\pi = 4015$ Hz. In Fig. 4a we have plotted calculated (full lines) and experimental (dotted lines) spectra for this case. The parameters and the additional line broadening have been taken to be the same as for the case $p = 1$ in Fig. 2. In Fig. 4b the spectra are shown without the Lorentzian broadening. One can see that the spectra around the second rotational resonance have a more complicated structure than in the $p = 1$ case. Still, there are two bands separated by the frequency equal to the corresponding offset from exact reso-

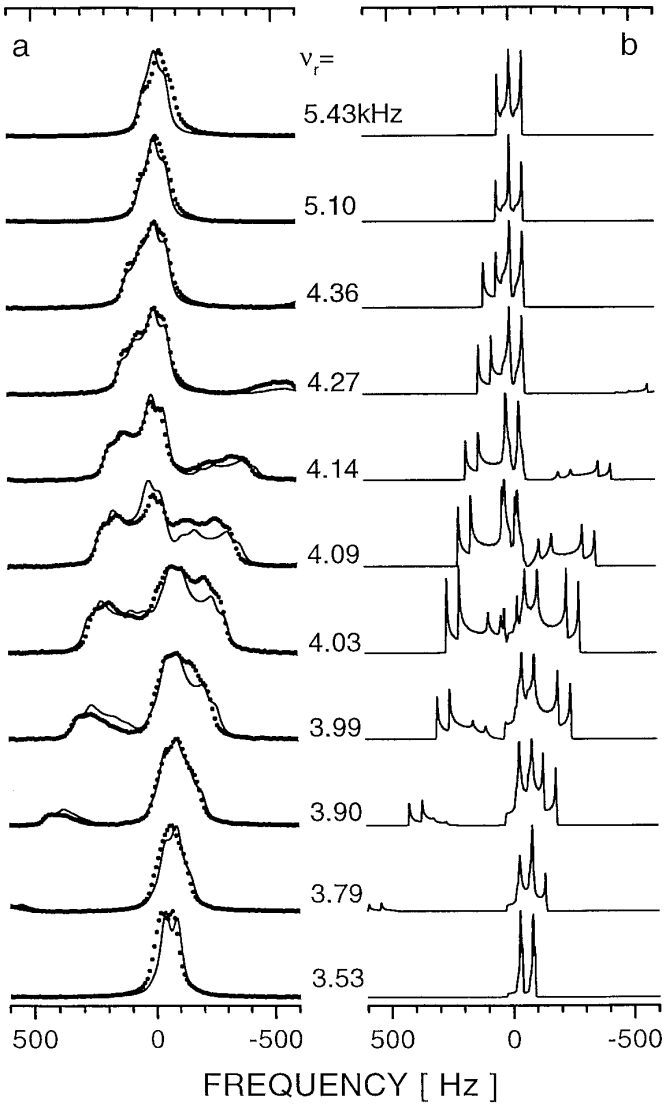

FIG. 4. ^{13}C MAS NMR spectra of the methyl carbon in ^{13}C-enriched Zn-acetate as a function of sample spinning frequency, ν_r, around the second rotational resonance. The same sample and parameters were used as given in the legend to Fig. 2. (a) Observed (dotted lines) and calculated (full lines) spectra. A common Lorentzian half-width of 20 Hz was convoluted in the calculated spectra. (b) Calculated spectra without additional broadening.

nance, $\Delta_L - 2\omega_r$. The agreement between simulation and experiment is relatively good, although in details the differences are larger than in the $p = 1$ case, especially at spinning rates close to the exact resonance. This may be caused by partial violation of the fast spinning condition in Eq. [16]. Additional errors can occur due to the always existing rotational sidebands which overlap the main lines near the rotational resonance and are not taken into account in the calculations. Nevertheless we wanted to give the detailed lineshape behavior also for this case. In Fig. 5 we have plotted the powder patterns as a function of the size of the anisotropy of the CSI for the two mutual orientations of the CSI and DI tensors at $\mu = 0$ and $\mu = 90°$ in the case of exact second rotational resonance. As before we have considered the case when the CSI anisotropy of one nucleus in the pair essentially exceeds that of the second nucleus. Compared to the case at the first rotational resonance, the lineshapes at the second rotational resonance are extremely sensitive to the particular set of the parameters of the relevant CSI tensor.

In addition to the peak always present at $\Delta_{20} = \pm\omega_D/8$, as in the case of pure DI [see Refs. (*5, 19*)], the other singularities noted in the figure appear at the following frequencies:

(a) case $\mu = 0°$

$$\Delta_{2a} = \left| \frac{1}{8}\,\omega_D\,\frac{1+4c}{16c^2}\,\sqrt{(1+4c)^2 + \left(4d - \frac{d}{c}\right)^2} \right|, \qquad [34]$$

where the parameters c and d are given by Eq. [26] and the singularity exists if

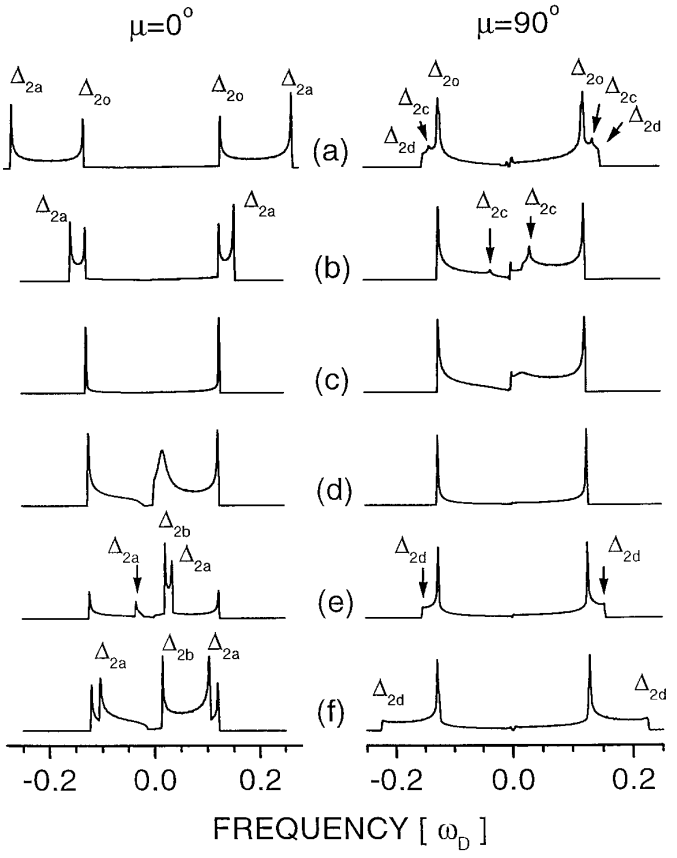

FIG. 5. Typical powder patterns of the coupled spin pair exactly at the second rotational resonance as a function of the magnitude of the anisotropy of the relevant CSI tensor at two Euler angles μ between the z-axes of the CSI and DI tensors. The positions of the noted singularities are given in the text. The model parameters: $\Delta_L/2\pi = 8.0$ kHz, $\omega_D/2\pi = 2.0$ kHz, $\eta^{(I)} = 0$, $\delta^{(S)} = 0$, $\omega_J = 0$. (a) $\delta^{(I)} = 250$ ppm; (b) $\delta^{(I)} = 100$ ppm; (c) $\delta^{(I)} = 50$ ppm; (d) $\delta^{(I)} = -50$ ppm; (e) $\delta^{(I)} = -100$ ppm; (f) $\delta^{(I)} = -200$ ppm.

$$c \le -\frac{1}{8} - \sqrt{\left(\frac{3}{8}\right)^2 - \left(d - \frac{\sqrt{2}}{4}\right)^2}, \quad \text{or } c \ge \frac{1}{4}; \quad [35]$$

$$\Delta_{2b} = \left|\frac{1}{8}\,\omega_D\,\frac{(1+4c)d}{4c^2}\right|, \quad [36]$$

and the singularity exists if

$$c \le -\frac{1}{8} - \sqrt{\left(\frac{3}{8}\right)^2 - \left(d - \frac{\sqrt{2}}{4}\right)^2}. \quad [37]$$

(b) case $\mu = 90°$

$$\Delta_{2c} = \left|\frac{1}{8}\,\omega_D\,\frac{4c-1}{16c}\sqrt{(4c-1)^2 + \left(4d + \frac{d}{c}\right)^2}\right|, \quad [38]$$

which exists if

$$c \ge \frac{1}{8} + \sqrt{\left(\frac{3}{8}\right)^2 - \left(d - \frac{\sqrt{2}}{4}\right)^2}, \quad \text{or } -\frac{1}{2} \le c \le -\frac{1}{4}; \quad [39]$$

$$\Delta_{2d} = \left|\frac{1}{8}\,\omega_D\left(c - \frac{1}{2}\right)^2\sqrt{\frac{1}{c(c-1)}}\right|, \quad [40]$$

which exists if

$$c \ge \frac{1+\sqrt{2}}{2}, \quad \text{or } c \le -\frac{1}{2}. \quad [41]$$

Although the formulae for the second resonance are more complex than those for the first resonance, they may turn out to be instructive for estimates of the CSI from the powder shape at the second rotational resonance.

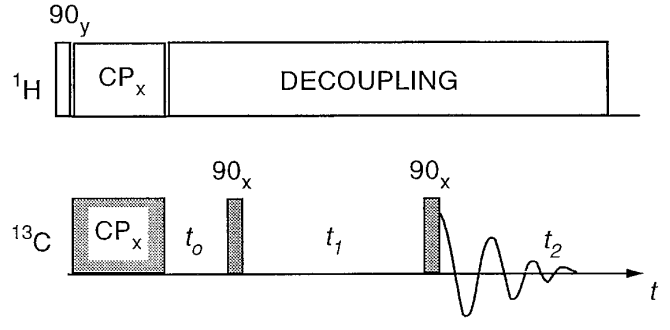

FIG. 6. Pulse sequence for the 2D polarization exchange experiment. After the cross-polarization pulse CP the magnetization vectors of the two coupled ^{13}C nuclei obtain opposite directions during the interval $t_0 = \pi/\Delta_L$, and after that the vectors are flipped to the z-axis by a 90° pulse. Polarization exchange takes place during the evolution time t_1 and the spectrum is recorded after a 90° detection pulse.

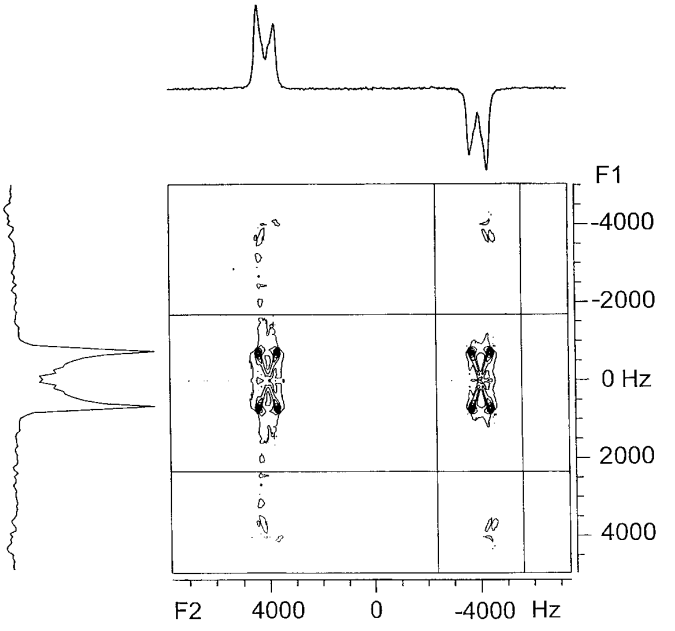

FIG. 7. 2D polarization exchange spectrum of doubly ^{13}C-labeled Zn-acetate at the first rotational resonance.

2D SPECTRA OF POLARIZATION EXCHANGE

Examination of Eqs. [A5] and [A7] makes it clear that in order to register the polarization exchange phenomena in a coupled spin pair the most promising approach is to utilize the process in the third subspace [A6]. Polarization vector evolution and thus the polarization exchange in this subspace begins as soon as the vector component proportional to I_z is not equal to that of S_z (see [A10]). Customarily a 2D experiment contains the preparation, evolution, and registration stages. Naturally, it is desirable to make the difference between the polarization vector I_z and S_z components as large as possible at the beginning of the evolution period and, at the same time, to localize the whole polarization vector in the third subspace. Figure 6 presents one of such pulse sequences we have used for this purpose. Here after the cross-polarization a suitably delayed $\pi/2$ pulse ($\Delta_L t_0 = \pi/2$) turns the I and S nuclear magnetizations along and opposite to the direction of the external magnetic field, respectively. During the evolution period t_1 polarization exchange between the two nuclei takes place, which is recorded after the readout pulse during t_2. In fact a similar manipulation of the spin system for polarization exchange study was proposed earlier by Raleigh *et al.* (*23*), where the antiparallel magnetization was created by selectively inverting one of the paired spins. The 2D spectrum obtained by

such a pulse sequence at the first rotational resonance from the doubly ^{13}C-labeled Zn-acetate is given in Fig. 7. As one can see, the contour plots for the two coupled nuclei have almost identical shape. The sum of the spectra in the vertical direction looks like a usual 1D spectrum at rotational resonance, except that the CH_3 line is inverted. The spectrum in the horizontal direction around the CH_3 resonance shows a symmetrical pattern with the splitting about twice as large as in the 1D spectrum.

With the universal rules for the polarization vector evolution presented in the Appendix one can get a theoretical description of the 2D spectrum obtained by this experiment. We start from the polarization vector after the preparation period in the form

$$\rho_{\text{preparation}} \propto -I_Z + S_Z + \frac{s}{c}\sum \kappa_j \Theta_j, \qquad [42]$$

where Θ_j denotes all the remaining spin-space base operators (see Appendix); the absolute value of the coefficient κ_j is smaller than 1 and the coefficients s and c have the meaning

$$s = \sin \Delta_p t_0,$$
$$c = \cos \Delta_p t_0. \qquad [43]$$

One can show that the polarization vectors of all the crystallites are localized in the third subspace only if

$$\pi \frac{\Delta_p}{\Delta_L} \ll 1. \qquad [44]$$

In this case the spectra in the ω_1 dimension reflect the polarization exchange phenomena in the third subspace and the spectra in the ω_2 dimension present the ordinary MAS NMR spectra. A complete analysis of this experiment shows that the full spectrum in the ω_1 dimension appears at the following frequencies:

(a) $\frac{p}{2}\omega_r + l\Delta_p + m\frac{1}{2}\omega_J$ and $\frac{3p}{2}\omega_r + l\Delta_p + m\frac{1}{2}\omega_J$,

where $l, m = \pm 1$;

(b) $p\omega_r + l2\Delta_p$ and $2p\omega_r + l2\Delta_p$,

where $l = -1, 0, 1$;

(c) 0 and $2\Delta_p$.

Here we must point out that the amplitudes of the terms (a) and (b) are proportional to the value of the parameter s in Eq. [43], which in usual cases is small. Therefore the low-frequency terms of the signal in band (c) merit our interest first of all.

This part of the signal in the vicinity of $\omega_L^{(I)}$ is collected into the following formula:

$$\begin{aligned} S^{(I)} \propto & -\sum_{l=\pm 1} l\frac{1}{2}\left\{\left(1-\frac{\Delta_Z^{(p)}}{\Delta_p}\right)\left[\left(1+\frac{\Delta_Z^{(p)}}{\Delta_p}\right)-\frac{1}{2}\left(\frac{\mathrm{Im}(K_p)}{\Delta_p}\right)^2\right]\sin 2\Delta_p t_1\right\} \\ & \times \cos\frac{1}{2}\omega_J t \cos(\omega_L^{(I)} - \Delta_p^{(r)} + l\Delta_p)t \\ & -\sum_{l=\pm 1}\left\{l\frac{1}{2}\frac{\Delta_Z^{(p)}}{\Delta_p}\left(1+l\frac{\Delta_Z^{(p)}}{\Delta_p}\right)^2 + \frac{K_p K_p^*}{\Delta_p^2}\left(1+l\frac{1}{2}\frac{\Delta_Z^{(p)}}{\Delta_p}\right)\cos 2\Delta_p t_1\right\} \\ & \times \cos\frac{1}{2}\omega_J t \sin(\omega_L^{(I)} - \Delta_p^{(r)} + l\Delta_p)t. \end{aligned} \qquad [45]$$

Naturally, in the receiver coil there are also induced the signal components of $S^{(S)}$ at frequencies around $\omega_L^{(S)}$. The formula determining the $S^{(S)}$ components can be obtained from Eq. [45] by changing the sign of the second term and substituting the factors $\cos/\sin(\omega_L^{(I)} - \Delta_p^{(r)} + l\Delta_p)t$ by $\cos/\sin(\omega_L^{(S)} + \Delta_p^{(r)} - l\Delta_p)t$, respectively.

Equation [45] does not describe the signal induced in the receiver coil by a single coupled spin pair, but provides the sum of the signals from two coupled spin pairs oriented at angles (β, γ) and $(180° - \beta, 180° + \gamma)$ in the rotor-fixed frame, respectively. Such simplification is always justified for a randomly oriented powder. The formula for a single pair in a single crystal is more complicated, involving phase distortions.

Numerical simulation of the 2D spectrum starting from Eq. [45] is not very convenient, because it needs as many powder averages as the number of data points in the simulated 2D array of FIDs. It is more expedient to use expressions where the complex Fourier analysis has already been performed analytically. As a result, one gets six different (complex) amplitudes generated by a coupled spin pair (β,

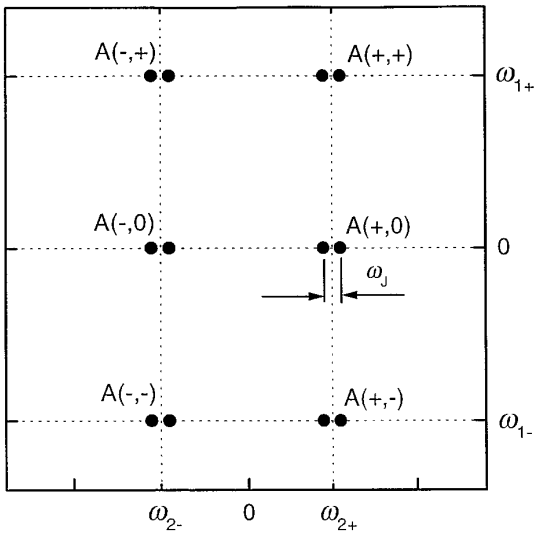

FIG. 8. Schematic illustration of the peak positions and amplitudes in the 2D polarization exchange spectrum generated by a coupled spin-$\frac{1}{2}$ pair and its co-oriented pair (see text). The splitting of the resonance lines by ω_J due to SSI occurs only in the ω_2 dimension.

γ) and its copair ($180° - \beta$, $180° + \gamma$) together as depicted in Fig. 8. The SSI induces additional splitting of the resonance lines by ω_J, but only in the ω_2 dimension. The nonzero amplitudes are generated at points with the coordinates in the 2D frame,

$$\omega_1 = 0 \quad \text{and} \quad \omega_{1\pm} = \pm 2\Delta_p \qquad [46]$$

in the ω_1 dimension, and at

$$\omega_{2\pm} = \Delta_p^{(r)} \pm \Delta_p \qquad [47]$$

in the ω_2 dimension, which is additionally split by $\pm\frac{1}{2}\omega_J$, and related to $\omega_L^{(I)}$. The amplitudes (see Fig. 8) are evaluated as

$$A(\pm, \pm) \propto i\left[\left(3 \pm \frac{\Delta_Z^{(p)}}{\Delta_p}\right)\frac{K_p K_p^*}{\Delta_p^2} - \frac{1}{2}\left(1 - \frac{\Delta_Z^{(p)}}{\Delta_p}\right)\left(\frac{\mathrm{Im}(K_p)}{\Delta_p}\right)^2\right]e^{i\varphi_D},$$

$$A(\pm, 0) \propto \mp i2\,\frac{\Delta_Z^{(p)}}{\Delta_p}\left(1 \mp \frac{\Delta_Z^{(p)}}{\Delta_p}\right)^2 e^{i\varphi_D},$$

$$A(\pm, \mp) \propto i\left[\left(1 \mp \frac{\Delta_Z^{(p)}}{\Delta_p}\right)\frac{K_p K_p^*}{\Delta_p^2} + \frac{1}{2}\left(1 - \frac{\Delta_Z^{(p)}}{\Delta_p}\right)\left(\frac{\mathrm{Im}(K_p)}{\Delta_p}\right)^2\right]e^{i\varphi_D}, \qquad [48]$$

where φ_D is the detector phase angle and either upper or lower signs must be selected.

The spectrum in the vertical direction $I(\omega_2)$ exactly coincides with the ordinary MAS NMR spectrum:

$$I(\omega_{2\pm}) \propto i\left(1 \mp \frac{\Delta_Z^{(p)}}{\Delta_p}\right)e^{i\varphi_D}. \qquad [49]$$

The spectrum in the horizontal direction $I(\omega_1)$ is symmetric,

$$I(\omega_{1+}) = I(\omega_{1-}) \propto i\left(1 - \frac{\Delta_Z^{(p)}}{\Delta_p}\right)\left(1 + \frac{\Delta_Z^{(p)}}{\Delta_p}\right)e^{i\varphi_D}$$

$$I(\omega_1 = 0) \propto i2\left(\frac{\Delta_Z^{(p)}}{\Delta_p}\right)^2 e^{i\varphi_D}, \qquad [50]$$

and, as already stated, it does not show the splitting caused by SSI.

Correct phasing of the experimental 2D spectra after the double Fourier transformation is not always an easy task. A somewhat better solution is to use in the second FT (complex Fourier analysis over the evolution time t_1) only the real part of the amplitudes obtained after the first FT (complex Fourier analysis over the registration time t_2). Such procedure has been applied for the spectrum presented in Fig. 7. In this case the amplitudes in the 2D spectra are as follows:

$$A(-, -) = A(-, +)^* \propto \left(1 + \frac{1}{2}\frac{\Delta_Z^{(p)}}{\Delta_p}\right) \times \frac{K_p K_p^*}{\Delta_p^2}\sin\varphi_D - i\,\frac{1}{2}\left[\left(1 - \frac{\Delta_Z^{(p)2}}{\Delta_p^2}\right) - \frac{1}{2}\left(1 - \frac{\Delta_Z^{(p)}}{\Delta_p}\right)\left(\frac{\mathrm{Im}(K_p)}{\Delta_p}\right)^2\right]\cos\varphi_D,$$

$$A(+, -) = A(+, +)^* \propto \left(1 - \frac{1}{2}\frac{\Delta_Z^{(p)}}{\Delta_p}\right) \times \frac{K_p K_p^*}{\Delta_p^2}\sin\varphi_D + i\,\frac{1}{2}\left[\left(1 - \frac{\Delta_Z^{(p)2}}{\Delta_p^2}\right) - \frac{1}{2}\left(1 - \frac{\Delta_Z^{(p)}}{\Delta_p}\right)\left(\frac{\mathrm{Im}(K_p)}{\Delta_p}\right)^2\right]\cos\varphi_D,$$

$$A(\mp, 0) \propto \pm\,\frac{\Delta_Z^{(p)}}{\Delta_p}\left(1 \pm \frac{\Delta_Z^{(p)}}{\Delta_p}\right)^2 \sin\varphi_D. \qquad [51]$$

It is easy to see that the amplitudes in the spectra in the present case do not differ essentially from those in the preceding variant of the calculation procedure. Indeed, in order to be valid one needs only to substitute the factors $ie^{i\varphi_D}$ in Eqs. [49] and [50] by $\sin\varphi_D$.

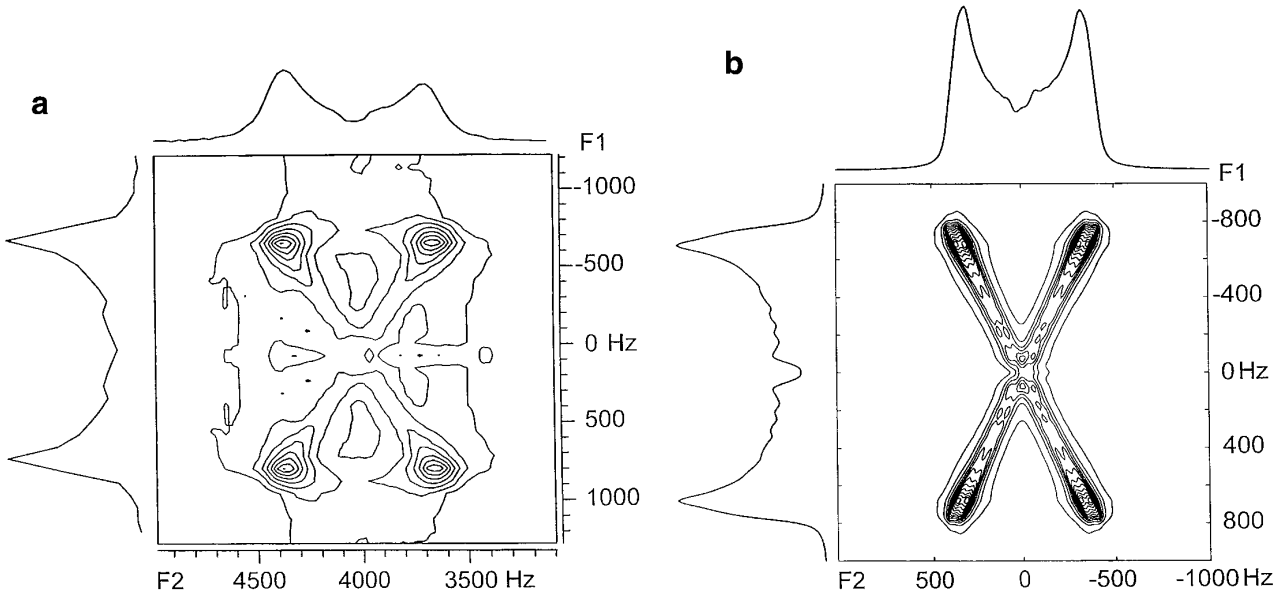

FIG. 9. Experimental (a) and simulated (b) 2D polarization exchange spectrum of the carboxyl carbon site of doubly ^{13}C-labeled Zn-acetate at the first rotational resonance.

In Fig. 9a we have given the 2D polarization exchange spectrum of the CH_3 resonance at the first rotational resonance observed in doubly ^{13}C-labeled Zn-acetate. The simulated spectrum given in Fig. 9b is obtained for the case $p = 1$ using the formulae [51] and the CSI and DI tensor parameters for Zn-acetate as given before for Fig. 2. It is obvious that the calculated spectrum reproduces comparatively well the experimental spectrum, although the splitting due to the SSI in the experimental spectrum is not resolved. This may be due to the deviation of the sample spinning frequency from exact resonance, because in this comparatively long experiment the stability of the sample speed was not better than ± 15 Hz. On the other hand, stability of the spinning frequency is not very critical to the spectrum in the F_1 ($\omega_1/2\pi$) dimension, because the polarization exchange frequency $2\Delta p$ depends only weakly upon the deviation from exact resonance. A similar comparison is carried out also at the second rotational resonance ($p = 2$) presented in Fig. 10. Here the spectra in the F_1 dimension contain a peak at zero frequency and two maxima at both sides of the zero-frequency peak. The low-frequency peak in full analogy to the 1D spectrum at the second rotational resonance (see Figs. 4 and 5b) indicates the contribution from the CSI term.

CONCLUSIONS

We have shown that the average Hamiltonian theory can be successfully applied to describe the MAS NMR spectra of a dilute homonuclear spin-$\frac{1}{2}$ pair over a broad region of sample spinning rates, including the exact rotational resonances. Comparison of the simulated spectra with the spectra recorded by the MAS NMR technique from polycrystalline samples of doubly ^{13}C-labeled Zn-acetate demonstrates excellent agreement for the spinning rates around the first rotational resonance. The agreement of the spectra around the second rotational resonance is not perfect, but good. The differences between simulated and calculated spectra in this case can be caused by some violation in our experiment of the fast spinning condition. In addition, the vector formalism developed here enables one to describe the 2D spectra of polarization exchange between the coupled nuclei. A reasonable agreement between the calculated and experimental 2D spectra shows that this type of experiment can be very useful in structural studies, where the lineshape analysis of ordinary rotational resonance spectra is not possible.

APPENDIX

The $\mathbf{H}^{(p)}$-induced motion of the state vector ρ in spin space may be described by the equation

$$\rho_T(t) = \mathbf{L}(\mathbf{H}^{(p)})\rho(0), \qquad [A1]$$

where the matrix of the Liouville superoperator $\mathbf{L}(\mathbf{H}^{(p)})$ is determined by Eq. [21].

It appears that the 16-dimensional spin space splits into four independent subspaces in the sense that the vector components of different subspaces do not mix during the $\mathbf{H}^{(p)}$-induced motion of the polarization vector. Thus the 16×16 matrix of $\mathbf{L}$ may be written in the block-diagonal form

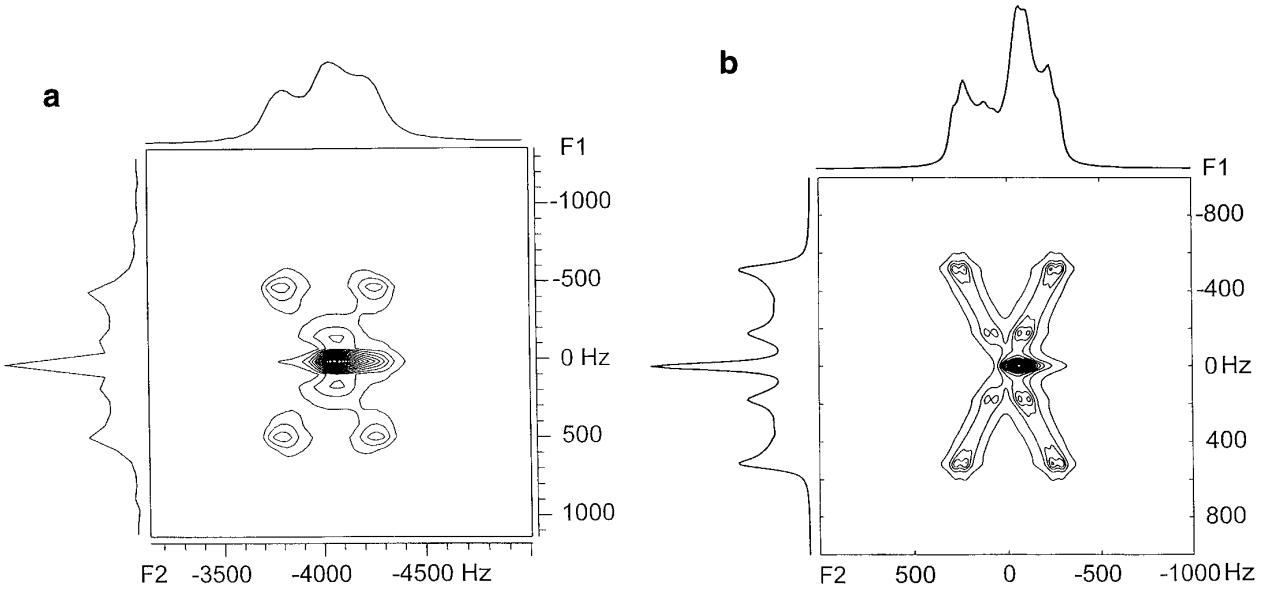

FIG. 10. Experimental (a) and simulated (b) 2D polarization exchange spectrum of the methyl carbon site of doubly ^{13}C-labeled Zn-acetate at the second rotational resonance.

$$\mathbf{L}(\mathbf{H}^{(p)}) = \begin{Vmatrix} \|\mathbf{L}^{(1)}\| & & & \\ & \|\mathbf{L}^{(2)}\| & & \\ & & \|\mathbf{L}^{(3)}\| & \\ & & & \|\mathbf{L}^{(4)}\| \end{Vmatrix}$$

and, equivalently to that, Eq. [A1] may be substituted by

$$\rho_{\mathrm{T}}(t) = \sum_{i=1}^{4} \mathbf{L}^{(i)}(\mathbf{H}^{(p)})\rho^{(i)}(0), \qquad [A2]$$

where $\mathbf{L}^{(i)}$ and $\rho^{(i)}(0)$ denote in the ith subspace operating Liouville superoperator and the state vector component, belonging to that subspace, respectively.

Now, making use of the spin operator set

$$(i = 1) \rightarrow (\mathbf{I}_+, \mathbf{I}_+\mathbf{S}_{\mathrm{Z}}, \mathbf{I}_{\mathrm{Z}}\mathbf{S}_+, \mathbf{S}_+) \qquad [A3]$$

as the base operators of the first subspace in the succession given above and the set of spin operators

$$(i = 2) \rightarrow (\mathbf{I}_-, \mathbf{I}_-\mathbf{S}_{\mathrm{Z}}, \mathbf{I}_{\mathrm{Z}}\mathbf{S}_-, \mathbf{S}_-) \qquad [A4]$$

as the base operators of the second subspace in the given succession, the matrices of the Liouville superoperators $\mathbf{L}^{(1)}$ and $\mathbf{L}^{(2)}$, operating in the first and the second subspace, are defined by the equations

$$\|\mathbf{L}^{(1)}\| = \begin{Vmatrix} N_1 & \frac{1}{4}N_2 & -\frac{1}{4}N_3^* & N_4^* \\ N_2 & N_1 & N_4^* & -N_3^* \\ N_3 & N_4 & N_1^* & -N_2^* \\ N_4 & \frac{1}{4}N_3 & -\frac{1}{4}N_2^* & N_1^* \end{Vmatrix},$$

$$\|\mathbf{L}^{(2)}\| = \|\mathbf{L}^{(1)}\|^*, \qquad [A5]$$

where

$$N_1 = \left(\cos \Delta_p t + i \frac{\Delta_{\mathrm{Z}}^{(p)}}{\Delta_p} \sin \Delta_p t\right) \cos \frac{1}{2} \omega_{\mathrm{J}} t,$$

$$N_2 = 2\left(\frac{\Delta_{\mathrm{Z}}^{(p)}}{\Delta_p} \sin \Delta_p t - i \cos \Delta_p t\right) \sin \frac{1}{2} \omega_{\mathrm{J}} t,$$

$$N_3 = -i2 \frac{K_p^*}{\Delta_p} \sin \Delta_p t \cos \frac{1}{2} \omega_{\mathrm{J}} t,$$

$$N_4 = -\frac{K_p^*}{\Delta_p} \sin \Delta_p t \sin \frac{1}{2} \omega_{\mathrm{J}} t.$$

In the case when the third subspace operator set

$$(i = 3) \rightarrow (\mathbf{I}_{\mathrm{Z}}, \mathbf{I}_+\mathbf{S}_-, \mathbf{I}_-\mathbf{S}_+, \mathbf{S}_{\mathrm{Z}}) \qquad [A6]$$

is used as the base of that spin space and retaining the succession as in [A6], the matrix $\|\mathbf{L}^{(3)}\|$ may be expressed in the following way:

$$\|\mathbf{L}^{(3)}\| = \begin{Vmatrix} N_5 & N_8 & N_8^* & N_{10} \\ N_7 & N_6 & N_9 & -N_7 \\ N_7^* & N_9^* & N_6^* & -N_7^* \\ N_{10} & -N_8 & -N_8^* & N_5 \end{Vmatrix}. \quad [A7]$$

Here

$$N_5 = \left[1 - \frac{K_p K_p^*}{2\Delta_p^2}(1 - \cos 2\Delta_p t)\right],$$

$$N_6 = \frac{1}{2}\left\{1 - \left(\frac{\Delta_Z^{(p)}}{\Delta_p}\right)^2 + \left[1 + \left(\frac{\Delta_Z^{(p)}}{\Delta_p}\right)^2\right] \times \cos 2\Delta_p t + i2\frac{\Delta_Z^{(p)}}{\Delta_p}\sin 2\Delta_p t\right\}$$

$$N_7 = \frac{K_p}{2\Delta_p}\left[\frac{\Delta_Z^{(p)}}{\Delta_p}(1 - \cos 2\Delta_p t) - i \sin 2\Delta_p t\right],$$

$$N_8 = \frac{K_p^*}{2\Delta_p}\left[\frac{\Delta_Z^{(p)}}{\Delta_p}(1 - \cos 2\Delta_p t) - i \sin 2\Delta_p t\right],$$

$$N_9 = \frac{1}{2}\left(\frac{K_p}{\Delta_p}\right)^2(1 - \cos 2\Delta_p t),$$

$$N_{10} = \frac{K_p K_p^*}{2\Delta_p^2}(1 - \cos 2\Delta_p t).$$

In the fourth subspace with the basis of the operator set

$$(i = 4) \rightarrow (\mathbf{I}_Z\mathbf{S}_Z, \mathbf{I}_+\mathbf{S}_+, \mathbf{I}_-\mathbf{S}_-, \mathbf{1}), \quad [A8]$$

the Liouville superoperator is representated by the unit matrix

$$\mathbf{L}_{k,j}^{(4)} = \begin{cases} 1, & k = j \\ 0, & k \neq j. \end{cases} \quad [A9]$$

In addition, let it be noted that

$$[\mathbf{H}^{(p)}, a\mathbf{I}_Z + b\mathbf{S}_Z] = (b - a)(K_p\mathbf{I}_+\mathbf{S}_- - K_p^*\mathbf{I}_-\mathbf{S}_+), \quad [A10]$$

and $\mathbf{H}^{(p)}$ does not cause the departure of the polarization vector from its thermal equilibrium state. As soon as $a \neq b$, evolution in the third subspace takes place.

ACKNOWLEDGMENT

This research was supported by grants from the Estonian Science Foundation.

REFERENCES

1. E. R. Andrew, S. Clough, L. F. Farnell, T. A. Gledhill, and I. Roberts, *Phys. Lett.* **21,** 505 (1966).
2. B. H. Meier and W. L. Earl, *J. Am. Chem. Soc.* **109,** 7937 (1987).
3. D. P. Raleigh, G. S. Harbison, T. G. Neiss, J. E. Roberts, and R. G. Griffin, *Chem. Phys. Lett.* **138,** 285 (1987).
4. T. G. Oas, R. G. Griffin, and M. H. Levitt, *J. Chem. Phys.* **88,** 629 (1988).
5. M. H. Levitt, D. P. Raleigh, F. Creuzet, and R. G. Griffin, *J. Chem. Phys.* **92,** 6347 (1990).
6. A. Kubo and C. A. McDowell, *J. Chem. Phys.* **93,** 7156 (1990).
7. T. Nakai and C. A. McDowell, *J. Chem. Phys.* **96,** 3452 (1992).
8. A. Schmidt and S. Vega, *J. Chem. Phys.* **96,** 2655 (1992).
9. R. Challoner, T. Nakai, and C. A. McDowell, *J. Chem. Phys.* **94,** 7038 (1991).
10. T. Nakai, R. Challoner, and C. A. McDowell, *Chem. Phys. Lett.* **180,** 13 (1991).
11. K. Eichele, G. Wu, and R. E. Wasylishen, *J. Magn. Reson. A* **101,** 157 (1993).
12. G. Wu and R. E. Wasylishen, *J. Magn. Reson. A* **102,** 183 (1993).
13. R. Challoner, C. A. McDowell, M. Yoshifuji, K. Toyota, and J. A. Tossell, *J. Magn. Reson. A* **104,** 258 (1993).
14. Z.-H. Gan and D. M. Grant, *Chem. Phys. Lett.* **168,** 304 (1990).
15. A. E. Bennett, L. R. Becerra, and R. G. Griffin, *J. Chem. Phys.* **100,** 812 (1994).
16. G. S. Spencer, K. W. Fishbein, M. H. Levitt, and R. G. Griffin, *J. Chem. Phys.* **100,** 5533 (1994).
17. J. H. Shirley, *Phys. Rev. B* **138,** 979 (1965).
18. U. Haeberlen and J. S. Waugh, *Phys. Rev.* **175,** 453 (1968).
19. E. Kundla and E. Lippmaa, *J. Chem. Phys.* **102,** 1569 (1995).
20. M. Goldman, *J. Magn. Reson. A* **102,** 173 (1993).
21. M. Edén, Y. K. Lee, and M. H. Levitt, *J. Magn. Reson. A* **120,** 56 (1996).
22. T. Nakai and C. A. McDowell, *Mol. Phys.* **88,** 1263 (1996).
23. D. P. Raleigh, M. H. Levitt, and R. G. Griffin, *Chem. Phys. Lett.* **146,** 71 (1988).